arXiv:1704.02151v1 [cond-mat.mtrl-sci] 7 Apr 2017

Topological nodal-line semimetals arising from crystal symmetry

Ryo Takahashi,[1] Motoaki Hirayama,[1,2] and Shuichi Murakami[1,2]

[1] *Department of Physics, Tokyo Institute of Technology, 2-12-1 Ookayama, Meguro-ku, Tokyo 152-8551, Japan*

[2] *TIES, Tokyo Institute of Technology, 2-12-1 Ookayama, Meguro-ku, Tokyo 152-8551, Japan*

(Dated: April 10, 2017)

Nodal-line semimetals, one of the topological semimetals, has line-shaped degeneracy (nodal line) where the gap is closed. Usually, nodal lines appear accidentally, and it is considered to be impossible to determine whether nodal lines appear from crystal symmetry alone. In this paper, we show that for spinless systems with certain space groups, presence of nodal lines results only from symmetry. We take a model Hamiltonian as an example and we show that it is always in a nodal-line semimetal phase, and the presence of the nodal line comes only from its space-group symmetry and time-reversal symmetry. We also establish a list of all the space groups, under which spinless systems always have nodal lines coming from symmetry, and illustrate where the nodal lines are located. We propose that Al_3FeSi_2 is one of the topological nodal-line semimetals arising from crystal symmetry.

PACS numbers: 71.15.-m, 61.50.Ah

I. INTRODUCTION

Discovery of topological insulators has triggered intensive studies on topology of electronic band structure of crystals.[1–6] After theoretical proposals, a number of materials are experimentally shown to be topological insulators.[7–9] In addition, a new topological phase called topological crystalline insulator has been proposed[10,11], and also experimentally confirmed.[12–14] In topological crystalline insulators, topological order is realized under some crystallographic symmetry. This is one of the examples of an interplay between topology and symmetry in crystals.

Through the research on topological insulators, a new concept of topological semimetals has been proposed[15–19]. In topological semimetals, the band gap closes at generic points in $\boldsymbol{k}$-space. In crystals, band degeneracy usually appears at high-symmetry points in $\boldsymbol{k}$-space. These degeneracy comes from crystal symmetry, and this is understood in terms of irreducible representations of space groups. On the other hand, some degenerate points between different bands appear by topological reasons. For example, Weyl semimetals have band degeneracy between conduction and valence bands at Weyl points which are located at general points in $\boldsymbol{k}$-space. This degeneracy is protected by band topology, not by symmetry.

Nodal-line semimetals, one of the topological semimetals, have line-shaped degeneracy called nodal line, where the gap is closed[20–26]. In general, appearance of nodal lines is not solely determined by symmetry. Therefore, such degeneracy can be removed without breaking symmetry in most cases. However, recent investigation have demonstrated that a nodal line is guaranteed to appear in certain spinful systems with non-symmorphic glide symmetry[27–29]. These nodal lines are called non-symmorphic nodal lines (NSNLs). While NSNLs in non-centrosymmetric spinful systems are systematically discussed in Ref. 27, little is known about NSNLs in spinless systems.

In this paper we theoretically show NSNLs in spinless systems with inversion and time-reversal symmetries. Inversion-symmetric crystals are abundant in nature and one can find various candidate materials. Moreover, nodal lines in spinless systems with both inversion and time-reversal symmetries are interesting, because they are always topological, characterized by π Berry phase around the nodal lines. This topological nature of the nodal lines gives their robustness against perturbations which break space-group symmetries. In this paper, we find that in some space groups, appearance of NSNLs is enforced by symmetry. In spinless systems with such space-group symmetries, when the filling factor is $4N + 2$ (N: integer) excluding spin degeneracy, the gap closes along the NSNLs. The origin of these NSNLs is non-commutativity in non-symmorphic glide symmetries of the space group. We find that NSNLs appear together with four-fold degenerated points and run through these points. We list all the space groups which have NSNLs enforced by symmetry. For example, a spinless system with $P4_2/mbc$ (No.**135**) crystal symmetry and time-reversal symmetry belongs to such semimetals. We construct a tight-binding model with this symmetry and show that in this system, nodal lines enforced by symmetry must appear and run through the A point, where the states are four-fold degenerate. We also show Al_3FeSi_2 as an example of this class of materials.

This paper is organized as follows. In Sec. II, we develop our theory of symmetry-protected NSNLs in spinless systems. In Sec. III, we show an example of NSNLs by constructing a model Hamiltonian and study properties of NSNLs. Section IV is devoted to the list of all the space groups with NSNLs enforced by symmetry in spinless systems. We also show how nodal lines emerge in each space group. In Sec. V, we show Al_3FeSi_2 as an example of such materials. Conclusion and discussions are given in Section VI. We assume presence of time-reversal symmetry and absence of the spin-orbit coupling

throughout the paper.

II. NON-SYMMORPHIC NODAL LINE ENFORCED BY SYMMETRY

Here, we explain basic ingredients of our theory on the NSNLs enforced by symmetry. Suppose non-interacting fermion systems with glide symmetry. The glide operation g is composed of a mirror operation σ and a half translation $\boldsymbol{t}$; $g = \{\sigma|\boldsymbol{t}\}$. On the glide-invariant plane in $\boldsymbol{k}$-space, the energy eigenstates are also eigenstates of the glide operator. Because of $g^2 = e^{-i\boldsymbol{k}\cdot\boldsymbol{t}}$, the glide eigenvalues are either $e^{-i\boldsymbol{k}\cdot\boldsymbol{t}/2}$ or $-e^{-i\boldsymbol{k}\cdot\boldsymbol{t}/2}$.

We will show a mechanism for emergence of a NSNL, which appears on the glide-invariant plane. We focus on 2-fold degeneracy on high-symmetry lines on the glide-invariant plane. This 2-fold degeneracy appears for some space groups with non-symmorphic glide symmetry. These double degeneracies on the high-symmetry lines are classified into two cases: glide eigenvalues ($= \pm e^{-i\boldsymbol{k}\cdot\boldsymbol{t}/2}$) being (i) the same or (ii) of opposite signs between the degenerate two bands. Here, we show that if on a single glide-invariant plane, the case (i) appears on one high-symmetry line and (ii) appears on another, a NSNL appears between these lines.

Figure 1 is a schematic figure of the NSNL. In Fig. 1(a), we assume that every energy band has 2-fold degeneracy along the two high-symmetry lines ℓ_1 and ℓ_2 on the glide-invariant plane in $\boldsymbol{k}$-space. On the line ℓ_1 (yellow), we assume that symmetry enforces the case (i), and double degeneracy with the same glide eigenvalues appears. On the other hand, on the line ℓ_2 (green), we assume that the case (ii) emerges, i.e., double degeneracy with glide eigenvalues of the opposite signs appears. We consider a curve C which connects between ℓ_1 and ℓ_2 lines as shown in Fig. 1(a). Along the curve C, the typical band structure is shown in Fig. 1(b). Here, because the curve C is on the glide-invariant plane, a glide eigenvalue for each band remain constant along C. Therefore, there should be a band crossing at an intermediate point $\boldsymbol{k}_C$ on the curve C, by which the glide eigenvalues are exchanged. The two bands do not anticross because of the difference in glide eigenvalues. Because this is true for an arbitrary curve C between ℓ_1 and ℓ_2 on the glide-invariant plane, the band degeneracy at $\boldsymbol{k}_C$ forms a nodal line. This nodal line, represented by the red dashed curve in Fig. 1(a), starts from the intersection between ℓ_1 and ℓ_2. If we set the Fermi energy so that two bands among four in Fig. 1(b) are filled, this nodal line is at or around the Fermi energy. In general, the energy is not constant along the nodal line. We emphasize that appearance of this nodal line is enforced by two different types of double degeneracies on ℓ_1 and ℓ_2. When the space group symmetry enforces the case (i) on ℓ_1 and (ii) on ℓ_2, perturbations cannot remove the nodal line. For example, even if the energies of the $(++)$ and $(--)$ doublets at $\boldsymbol{k}_1$ are interchanged by perturbation, the nodal line still persists.

Appearance of a NSNL in this example is guaranteed by 2-fold degenerate high-symmetry lines, one with the same glide eigenvalues, and the other with opposite glide eigenvalues. By considering various high-symmetry lines on the glide-invariant plane, positions of the nodal lines can be determined by symmetry. Four representative examples are shown in Figs. 2(a)-(d). In Figs. 2(a)-(d), the high-symmetry lines with the same glide eigenvalues are shown in yellow, and those with the glide eigenvalues of opposite signs are shown in green. The four corners in each panel represent different time-reversal invariant momenta. In (a)-(d), four-fold degenerate points (red points) appear at the intersection between the green and the yellow lines. The NSNL appears between the green and the yellow lines, and starts from the four-fold degenerate points. In (a)-(c), topology of the nodal lines is determined as dashed lines, whereas in (d) there are two possibilities for the nodal line, shown as dotted lines.

So far, we have discussed NSNLs appearing between two high-symmetry lines. Other types of NSNLs appear between two high-symmetry points, or between a high-symmetry point and a high-symmetry line, as shown in Figs. 2(e) and (f). Mechanism of appearance of this type of NSNLs is the same as that of the NSNL in Fig. 1(a) with replacing ℓ_1, ℓ_2 in Fig. 1(a) with two high-symmetry points or with a high-symmetry point and a high-symmetry line. The same argument as in Fig. 1(b) holds as long as the energy bands are 2-fold degenerated at the two ends of the curve C, one with the same glide eigenvalues, and the other with opposite glide eigenvalues.

However, in many cases, space-group symmetry alone does not guarantee appearance of NSNLs, because there are usually several options for combinations of glide eigenvalues on each high-symmetry line. Nevertheless, we show in the following that in some space groups, existence of the NSNL is guaranteed by the space-group symmetry. These space groups have limited combinations of glide eigenvalues, and on two lines ℓ_1 and ℓ_2 in $\boldsymbol{k}$-space, the glide eigenvalues are always as shown in Fig. 1(a). That makes a NSNL to be enforced by symmetry. From the list of irreducible representations of space groups[30], we can determine what kind of band degeneracy appears on high-symmetry lines.

III. MODEL CALCULATION

In this section, we introduce a tight-binding model which has NSNLs enforced by space-group symmetry. We show appearance of the NSNLs in this model, and see how it is robust against perturbations.

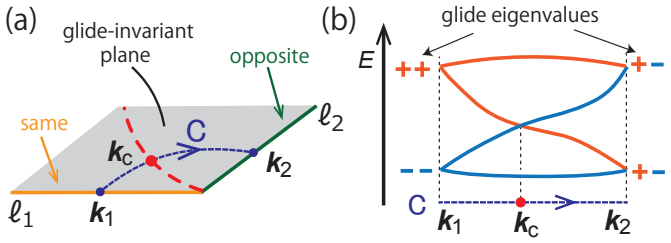

FIG. 1. (Color online) Mechanism of emergence of a NSNL. (a) Curve C which connects two high-symmetry lines ℓ_1 and ℓ_2 on a glide-invariant plane. Energy bands have 2-fold degeneracy along these lines. Glide eigenvalues of the doubly degenerate states are the same on ℓ_1 (yellow), and are of the opposite signs on ℓ_2 (green). A NSNL (red dashed line) appears between ℓ_1 and ℓ_2. (b) Schematic figure of the energy bands along the curve C. Glide eigenvalues are exchanged along the curve C, and a degeneracy appears at $\boldsymbol{k}_{\rm C}$. The signs $\pm$ denote the glide eigenvalues $\pm e^{-i\boldsymbol{k}\cdot\boldsymbol{t}/2}$.

TABLE I. Symmetry operations in $P4_2/mbc$ symmetry.

M_z	$(x,y,z) \to (x,y,-z)$
G_x	$(x,y,z) \to (-x,y,z) + (\frac{1}{2},\frac{1}{2},0)$
G_y	$(x,y,z) \to (x,-y,z) + (\frac{1}{2},\frac{1}{2},0)$
G_{x-y}	$(x,y,z) \to (y,x,z) + (\frac{1}{2},\frac{1}{2},\frac{1}{2})$
G_{x+y}	$(x,y,z) \to (-y,-x,z) + (\frac{1}{2},\frac{1}{2},\frac{1}{2})$
P	$(x,y,z) \to (-x,-y,-z)$

A. Tight-binding model with $P4_2/mbc$ symmetry and its band structure

We construct a tight-binding model whose space group is $P4_2/mbc$ (No.**135**), having mirror symmetry M_z, four glide symmetries $G_x, G_y, G_{x\pm y}$ and inversion symmetry P, as listed in Table I. This model is a spinless counterpart of the model proposed in Ref. 31. The model is constructed on a tetragonal crystal with four sub-lattices in the unit cell labeled by $(\tau_z, \mu_z) = (\pm 1, \pm 1)$ (Fig. 3(a)), and each sub-lattice has one state. Our tight-binding Hamiltonian is defined as follows:

$$\begin{aligned}\mathcal{H}(\boldsymbol{k}) &= t_{xy}\tau_x \cos\tfrac{k_x}{2}\cos\tfrac{k_y}{2} + t_z\mu_x\cos\tfrac{k_z}{2} \\ &+ t_a\tau_x\mu_x\cos\tfrac{k_x}{2}\cos\tfrac{k_y}{2}\cos\tfrac{k_z}{2} + t_b\mu_z(\cos k_x - \cos k_y) \\ &+ t_c\tau_z\mu_z \sin k_x \sin k_y, \end{aligned} \tag{1}$$

where t_{xy}, t_z, t_a, t_b, and t_c are real hopping amplitudes, and τ_i, μ_i are Pauli matrices acting on the sublattice degree of freedom. Here, the lattice constants along the three axes are set as unity for simplicity. Its band structure is shown in Fig. 3(c), where we set the parameters as $t_{xy} = 1.0$, $t_z = 0.5$, $t_a = t_b = t_c = 0.3$. We can see some degeneracy along the Γ-X and R-Z lines between the second and third bands in the band structure. These degeneracies are not limited to isolated points in $\boldsymbol{k}$-space but are a part of NSNLs. The NSNLs of this model are shown in Fig. 3(b). This model has two types of NSNLs; one is on the $k_z = \pi$ plane and the other is on $k_x = 0$ and on $k_y = 0$. The NSNLs on the mirror-invariant plane $k_z = \pi$ are shown as blue curves. They connect between the A points. On the glide-invariant planes $k_x = 0$ and $k_y = 0$, the NSNLs are shown as green curves. The appearance of these nodal lines are explained within our theory in the following.

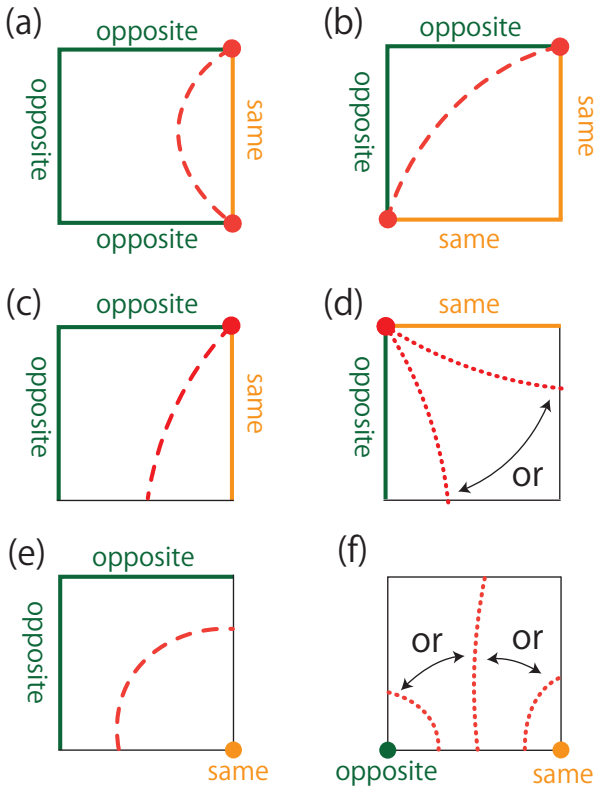

FIG. 2. (Color online) Six representative examples of NSNLs on a glide-invariant plane. Only a quarter of a two-dimensional slice of the three-dimensional Brillouin zone is shown, and the four corners represent different time-reversal invariant momenta (TRIM). Green and yellow heavy lines and points mean 2-fold degeneracy with opposite or same glide eigenvalues, respectively. In (a)-(d), four-fold degenerate points (red points) appear at the intersection of green and yellow lines. On the black thin lines, there is no band degeneracy coming from symmetry. Dashed or dotted red lines are NSNLs, and they should appear between a green line and a yellow line. In (a)-(c), topology of the NSNLs is determined as dashed lines, whereas in (d) there are two possibilities for the topology of the NSNL, shown as dotted lines. (e)-(f) NSNLs appear between a point and lines, or between two points. In (f), there are three possibilities for the topology of the NSNL, shown as dotted lines.

Before discussing the origin of NSNLs, we explain double degeneracy in the band structure of the model. Because of the symmetry, energy bands have 2-fold degeneracy along several high-symmetry lines such as X-M, X-R, M-A, A-R, and Z-A, as determined from the irreducible representations of the space group No.**135**[30]. For exam-

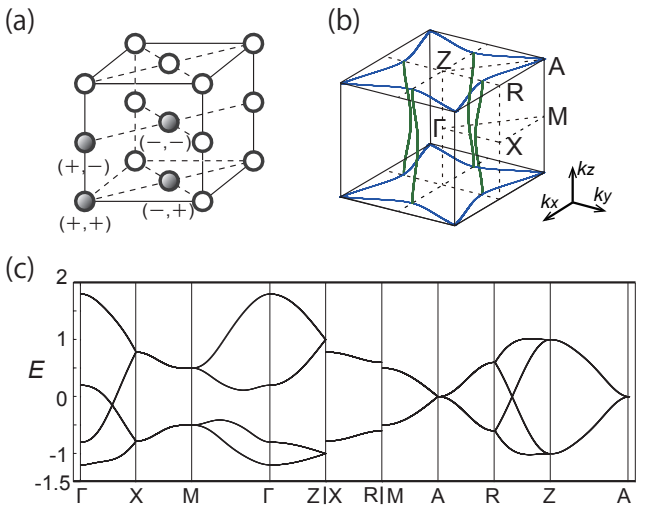

FIG. 3. (Color online) (a) Tetragonal crystal structure of our model. The four gray spheres denote the unit cell. (b) NSNLs of the model (1), shown in the Brillouin zone enclosed by the planes $k_i = \pm\pi$ $(i = x, y, z)$. There are two types of NSNLs, one in blue and the other in green. The NSNL on $k_z = \pi$ plane, drawn in blue, is enforced by symmetry, while the NSNLs on the planes $k_x = 0$ and $k_y = 0$ are not. (c) Band structure of the model (1). The parameters are $t_{xy} = 1.0,\ t_z = 0.5,\ t_a = t_b = t_c = 0.3$.

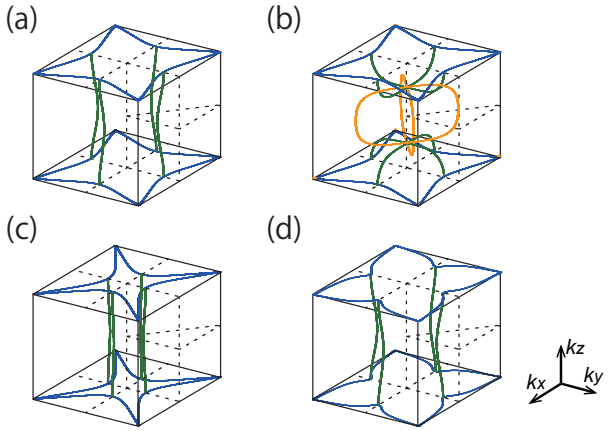

FIG. 4. (Color online) Positions of nodal lines of the model (1) for various values of the parameters. In (a), the values are $t_{xy} = 0,\ t_z = 0.5,\ t_a = t_b = t_c = 0.3$. In (b), only t_a is changed to $t_a = 1.5$. In (c), only t_b is changed to $t_b = 1.5$. In (d), only t_c is changed to $t_c = 1.5$. Colored lines are nodal lines. Only blue lines are NSNLs enforced by symmetry. In (b) additional nodal lines appear on the $k_x = \pm k_y$ planes, shown in yellow. They are not enforced by symmetry.

ple, there is only one two-dimensional irreducible representation along the Z-A line. It gives degeneracy between two states with the mirror eigenvalue of M_z being of opposite signs.

We now explain the origin of the NSNLs of the model. First, let us focus on $k_z = \pi$ plane, which is invariant under the mirror operation M_z. All the energy bands have 2-fold degeneracy along the A-R line and the Z-A line on the $k_z = \pi$ plane. Along the Z-A line, two Bloch states with opposite M_z eigenvalues are degenerate, corresponding to the case (ii). On the other hand, along the A-R line, two Bloch states with the same mirror M_z eigenvalue are degenerate, i.e. the case (i) emerges. Therefore, between the Z-A line and the A-R line, mirror eigenvalues M_z are exchanged, and a NSNL appears between them as shown in Fig. 1(a). We emphasize that appearance of this NSNL is enforced by symmetry. There is no other possibility of band degeneracy along the Z-A line and along the A-R line.

The origin of the double degeneracy is the non-commutative nature of the non-symmorphic glide symmetry. For example, along the Z-A line, the glide operation G_{x+y} anti-commutes with the mirror operation M_z, giving double degeneracy between states with opposite M_z eigenvalues. On the other hand, along the A-R line, the glide operation G_y anti-commutes with the product of time-reversal operation Θ and inversion operation P, giving double degeneracy between states with same M_z eigenvalues.

Next, we focus on the $k_x = 0$ plane, which is invariant under the glide operation G_x. Energy bands have 2-fold degeneracy along the X-R line and at the Z point. Along the X-R line, two Bloch states with opposite G_x eigenvalues are degenerate. On the other hand, at the Z point, two Bloch states with the same G_x glide eigenvalue are degenerated. Therefore between the X-R line and the Z point, glide eigenvalues are exchanged, and a NSNL must appear between them, as is similar to Fig. 2(e). Although the appearance of this NSNL is guaranteed by the double degeneracy along the X-R line and at the Z point, this NSNL is not enforced by symmetry in general. That is because there are several irreducible representations at the Z point, some of which do not enforce appearance of NSNLs. In other words, in general systems with the same symmetry, double degeneracy with opposite signs of G_x glide eigenvalues at the Z point is also allowed by symmetry, which does not enforce NSNLs. Therefore, general systems with the same symmetry may have no NSNL on the $k_x = 0$ plane.

B. Robustness of non-symmorphic nodal line

Thus, we have shown the NSNL on the $k_z = \pi$ plane appears only for a symmetry reason alone. That means this NSNL should appear independently of the values of the parameters of the Hamiltonian; hence, this NSNL must be robust against a change of parameters. In our model, we checked this by changing the three parameters t_a, t_b, t_c of the model Hamiltonian. In Fig. 4, we show the positions of the nodal lines for various values of the parameters t_a, t_b and t_c. We can see that the nodal lines on the $k_z = \pi$ move, but do not disappear when the parameters change.

Similarly, the NSNLs on the $k_x = 0$ plane and on the $k_y = 0$ plane are robust against a change of parameters. The reason is that because in this particular model, the glide eigenvalues are always exchanged between the X-R line and the Z point. Therefore, the NSNLs may move or change their topology, but never disappear.

However, there is a difference between the NSNL on the $k_z = \pi$ plane and the NSNLs on the $k_x = 0$ and $k_y = 0$ planes. The former is enforced by symmetry, but the latter is not. Therefore, in general systems with the same symmetry, the former always exists, but the latter may not exist.

IV. GENERALIZATION TO OTHER SPACE GROUPS

In this section, we generalize our results to other space groups that have inversion symmetry and glide (or mirror) symmetries. Time-reversal and inversion symmetries are assumed throughout our theory. It is a cumbersome task to find out the positions of the NSNLs enforced by symmetry for all the space groups, because there are varieties of $\boldsymbol{k}$-points and irreducible representations. We can facilitate this task by excluding space groups without NSNLs in the following way.

The NSNLs in our theory require two different types of 2-fold degeneracy along two axes on the glide- (mirror-) invariant plane; on one axis the glide (or mirror) eigenvalues are the same, and on the other they have the opposite signs. At the intersection of the axes, the bands are fourfold degenerate if a spin degree of freedom is neglected. If we include a spin degree of freedom, it causes 8-fold degeneracy at the intersection of two axes. This means that the minimal filling to realize a band insulator should be equal or larger than eight in candidate space-group symmetries. Here, we can use the theory by Watanabe, Po, Zaletel and Vishwanath, which recently showed a lower bound of the minimal insulating filling for 230 space groups[32]. From their work[32], the following 17 space groups, having inversion symmetry, are candidate space groups with symmetry-enforced NSNLs: **52**, **54**, **56**, **57**, **60**, **61**, **62**, **73**, **130**, **133**, **135**, **138**, **142**, **205**, **206**, **228** and **230**. By examining all these space groups, we find that the following 11 space groups have NSNLs enforced by symmetry: **52**, **54**, **56**, **57**, **60**, **61**, **62**, **130**, **135**, **138**, **205**. General systems with other space group symmetries have 8-fold degenerated points, but may not have NSNLs. In the following , we show the positions of the symmetry-enforced NSNLs for these space groups.

A. Orthorhombic primitive space group

In this section, we discuss systems with the following 7 orthorhombic space groups: No.**52**, **54**, **56**, **57**, **60**, **61** and **62**. These space groups have three glide symmetries with glide planes orthogonal to each other, three screw symmetries with screw axes orthogonal to each other, and inversion symmetry. Figure 5(a) shows 1/8 of the Brillouin zone. Along some of the edges of the 1/8 Brillouin zone, two glide operations with glide planes orthogonal to each other anti-commute: this occurs only when at least one component of the wavevector k_i $(i = x, y, z)$ is π. Therefore, two- or fourfold degeneracy appears along some of the edges of the 1/8 Brillouin zone. Emergence of NSNLs depends on geometric arrangement of degeneracy lines.

In Fig. 5(b1)-(h1), we illustrate geometric arrangement of high-symmetry lines with two- or fourfold degeneracy. Each high-symmetry line is invariant under two different glide operations. We label high-symmetry lines with 2-fold degeneracy as S if two Bloch states have same eigenvalues for at least one of the glide operations, and as OPP otherwise. We show high-symmetry lines with four-fold degeneracy as red double lines and labeled as DNLs (double nodal lines). The resulting nodal lines in these 7 space groups are illustrated in Fig. 5(b2)-(h2). These NSNLs have the features described in Sec. II: appearance of these NSNL is guaranteed by 2-fold degenerate high-symmetry lines, one with same glide eigenvalues, and the other with opposite glide eigenvalues. As a result of calculation, we find that all the NSNLs in these space groups cross at four-fold degenerated points. We illustrate these four-fold degenerated points as red points in Fig. 5(b2)-(h2). For convenience of readers, in Appendices A and B, we explain mechanism of emergence of four-fold degeneracy in orthorhombic and tetragonal primitive space groups.

B. Tetragonal primitive space group

In this section, we discuss the following 4 tetragonal space groups: No.**130**, **133**, **135** and **138**. Among them, we found that No.**133** do not have NSNLs enforced by symmetry. In spinless systems with the space group No.**133**, there are several choices of irreducible representations, and some of them do not have NSNLs. Therefore, general systems with space group No.**133** may not have NSNLs. As compared with orthorhombic space groups, in tetragonal space groups, additional four-fold screw symmetry doubles the number of symmetry operations, and additional glide-invariant planes along (110) and $(1\bar{1}0)$ appear. Along the Γ-Z and M-A lines, which are invariant under four-fold screw symmetry, there are various irreducible representations, due to the screw symmetries, and one cannot conclude existence of NSNLs from space-group symmetry alone. Therefore, we focus on other high-symmetry lines. In Fig. 6(b1)-(d1), we illustrate geometric arrangement of high-symmetry lines with two- or four-fold degeneracy other than the Γ-Z and M-A lines. In Fig. 6(b2)-(d2), we illustrate the location of NSNLs enforced by symmetry.

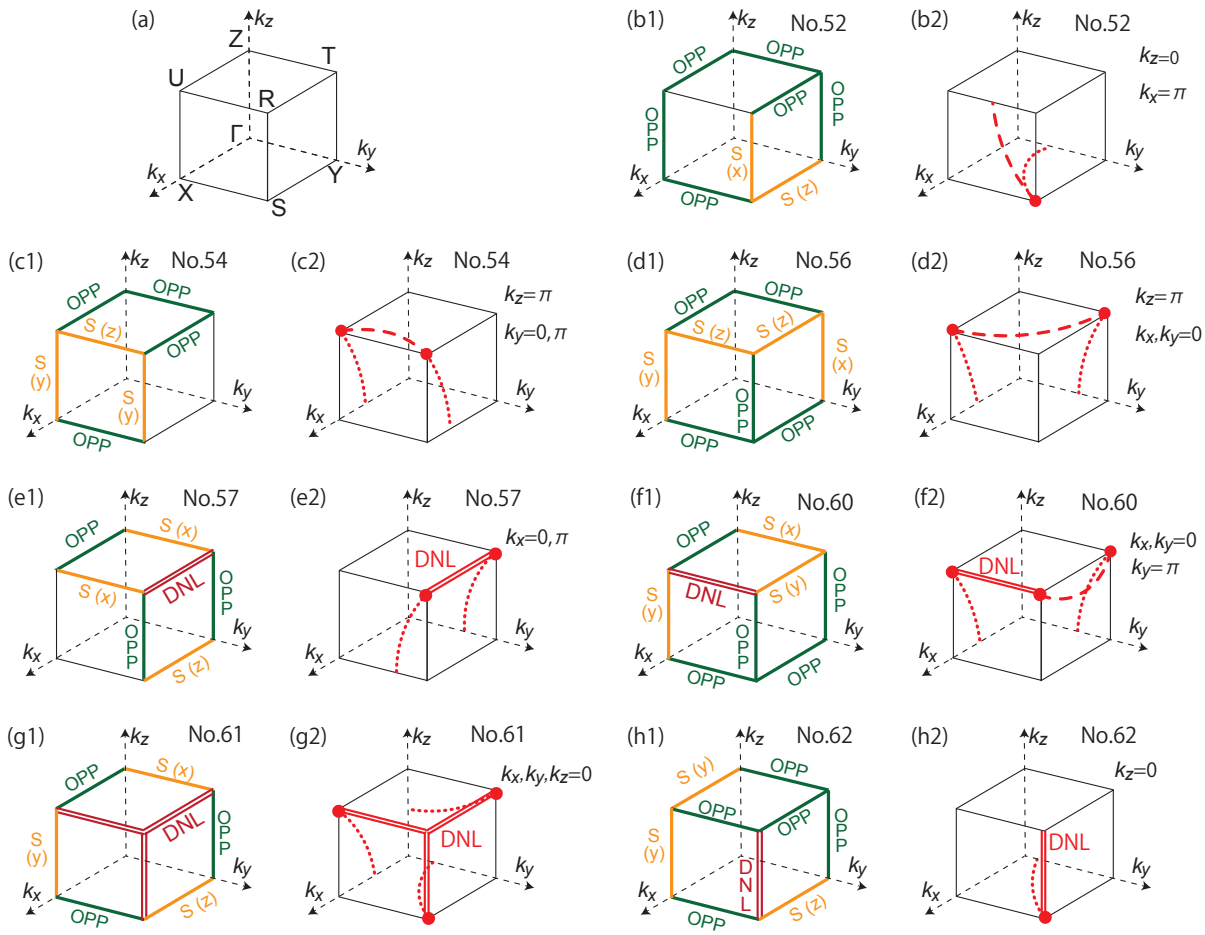

FIG. 5. Nodal lines in the orthorhombic space groups No.**52**, **54**, **56**, **57**, **60**, **61** and **62**. (a) Brillouin zone and symmetry labels for an orthorhombic primitive lattice. (b1)-(h1) Degeneracies along the high-symmetry lines and their glide eigenvalues, which correspond to high-dimensional irreducible representations. Yellow and green heavy lines mean 2-fold degeneracy with same and opposite glide eigenvalues, labeled with S (x, y, z) and OPP, respectively. S (x, y, z) means that glide eigenvalues whose glide plane is perpendicular to the x, y or z direction are the same between the degenerated two bands. Red double lines mean a double nodal line (DNL) having four-fold degeneracy. (b2)-(h2) NSNLs in these space groups. Dashed lines (red) and dotted lines (red) are NSNLs. Topology of the dotted nodal lines has more than one possibilities from symmetry alone (see Fig. 2(d)), and in the figures we only show one possibility for the positions of the nodal lines, as dotted lines.

C. Trigonal primitive space group

In this section, we discuss the trigonal space group No.**205**. Because the space group No.**61** is a subgroup of No.**205**, NSNLs in No.**205** are almost the same as those in No.**61**. In Fig. 7, we illustrate geometric arrangement of high-symmetry lines with two- or fourfold degeneracy, and locations of the NSNLs.

D. Non-primitive space group

In this section, we discuss systems with the following 5 non-primitive space groups: No.**73**, **142**, **206**, **228** and **230**. From the same analysis with that in Sec. I Ⅱ A-C, we found that these space groups do not have NSNLs enforced by symmetry. It is either because there are no 2-dimensional irreducible representations with the same glide eigenvalues, or because there are too many options of irreducible representations, depending on the space groups. For example, in the space group No.**73**, the three planes $k_{x,y,z} = 0$ are the only glide-invariant planes. Therefore, no 2-fold degeneracy appears with the same glide eigenvalues. Other examples are No.**142** and No.**228**, which have several choices of irreducible representations. Some of them enforce NSNLs, but others do not. Therefore, general systems with these space group symmetries may not have NSNLs.

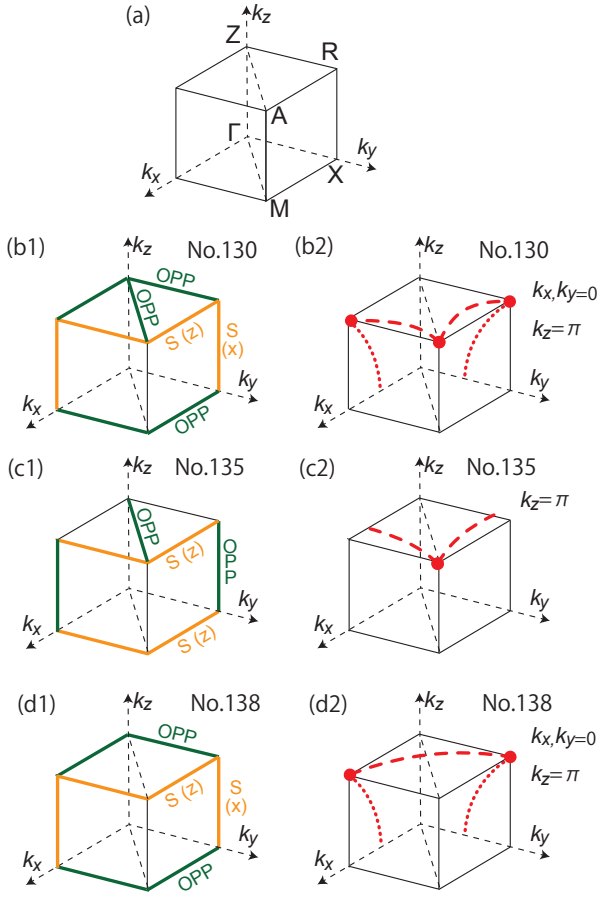

FIG. 6. (Color online) Nodal lines in the tetragonal space groups No.**130**, **135** and **138**. (a) Brillouin zone and symmetry labels for a tetragonal primitive lattice. (b1)-(d1) Degeneracies along the high-symmetry lines and their glide eigenvalues, which correspond to high-dimensional irreducible representations. (b2-h2) NSNLs in tetragonal space groups No.**130**, **135** and **138**. The notations are the same with those in Fig. 5.

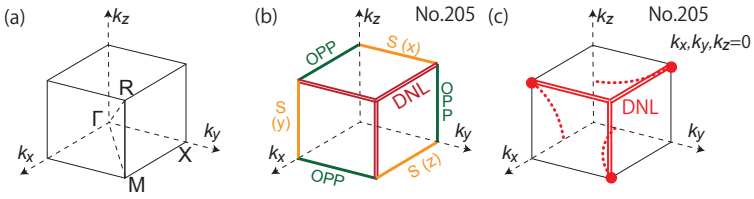

FIG. 7. (Color online) Nodal lines in the trigonal space group No.**205**. (a) Brillouin zone and symmetry labels for a trigonal primitive lattice. (b) Degeneracy along the high-symmetry lines and their glide eigenvalues, which corresponds to high-dimensional irreducible representations. (c) NSNLs in trigonal space group No.**205**. The notations are the same with those in Fig. 5.

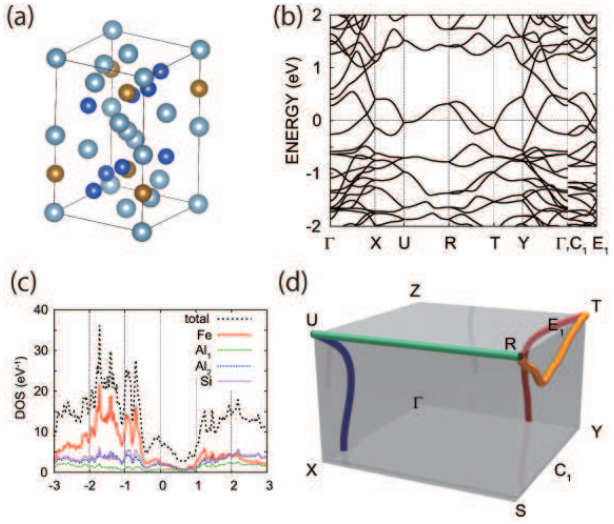

FIG. 8. (Color online) (a) Crystal structure of Al_3FeSi_2. The blue, grey, and yellow balls represent Si, Al, and Fe atoms, respectively. There are four Al_1 and eight Al_2 atoms in a unit cell, classified in terms of symmetry-equivalent positions. Al_1 atoms are located at positions with high symmetry, specifically (0,0,0),(0.5,0.5,0.5),(0,0,0.5),(0.5,0.5,0) in relative coordinates. (b) Electronic band structure of Al_3FeSi_2. The energy is measured from the Fermi level. C_1/E_1 is the midpoint of the Y-S/T-R line. (c) Total and partial density of states of Al_3FeSi_2. (d) Nodal lines around the Fermi level. The green line in the U-R line represents four-fold degeneracy, and the others represent 2-fold degeneracy.

V. SYMMETRY-ENFORCED NODAL LINES IN AL_3FESI_2

Thus far, we have found space groups with symmetry enforced NSNLs. Therefore, to find materials with such NSNLs, we should search for materials with the listed space groups with negligible spin-orbit coupling. Here, the fillings should be $(4N + 2)$ electrons per unit cell excluding spin degeneracy, where N is an integer. Here, we propose Al_3FeSi_2 to have symmetry-enforced NSNLs.

We calculate the band structures within the density functional theory using *ab initio* code OpenMX[33]. The electronic structure is calculated in the generalized gradient approximation (GGA). The $12\times12\times8$ regular **k**-mesh including the Γ point is employed for Al_3FeSi_2.

Al_3FeSi_2 is one of the materials with symmetry-enforced nodal lines. The space group of Al_3FeSi_2 is *Pbcn* (No. **60**) and the crystal structure is shown in Fig. 8(a)[34].

Figure 8(b) is the electronic structure of Al_3FeSi_2. We have checked that the system is non-magnetic in the spin-dependent calculation, reflecting a valley in the density of states near the Fermi level (Fig. 8(c)). The electronic band structure near the Fermi level originates from the Fe 3*d* orbitals hybridizing with orbitals from Al and Si. As shown in Fig. 8(a), the unit cell contains four Fe atoms surrounded by ten atoms with *p* orbitals (Al and Si) per one Fe atom, and all the Fe atoms are related by glide operation with each other. As shown in Fig. 8(b), the four bands are degenerate at the edge of the Brillouin zone $k_x = k_z = \pi$, i.e. the U-R line, regardless of the

value of k_y. This degeneracy originates from space-group symmetry and time-reversal symmetry as we discussed in Sec. IV. In other words, an orbital cannot make a bonding or anti-bonding state with the orbital in other sublattice cell when $k_x = k_z = \pi$. The nodal lines are shown in Fig. 8(d), which perfectly agree with our prediction in Fig. 5(f2).

VI. CONCLUSION AND DISCUSSION

In the present paper, we showed that in spinless systems with both inversion and time-reversal symmetries, symmetry-enforced NSNLs appear in specific space groups, when the filling factor is $4N+2$ (N: integer) excluding spin degeneracy. We listed all the space groups with NSNLs enforced by symmetry, and showed corresponding topology of nodal lines. In particular, in spinless systems, we found that NSNLs enforced by symmetry start from four-fold degenerate points. These results are confirmed for the tight-binding model with $P4_2/mbc$ (No.**135**) crystal symmetry and time-reversal symmetry. Symmetry-enforced NSNLs appear regardless of the values of the parameters of the Hamiltonian. We also showed that Al_3FeSi_2 is an example of materials with symmetry-enforced NSNLs. Our results are helpful in searching candidate materials with NSNLs.

Our results in the present paper stem from single-valued irreducible representations of the space groups. Therefore, these results can be applied to bosonic systems, such as photons, magnons, and phonons as well. Namely, in a bosonic systems, symmetry-enforced nodal lines are present only in the space groups **52**, **54**, **56**, **57**, **60**, **61**, **62**, **130**, **135**, **138**, **205**, and the positions of the symmetry-enforced nodal lines are shown in Figs. 5, 6, and 7. Systems with other space group symmetries may have nodal lines but they are not enforced by symmetry.

There are some earlier studies on NSNLs enforced by symmetry in spinful systems. In spinful systems, because of the difference of irreducible representations, the positions of the NSNLs are totally different from those in spinless systems discussed in the present paper. For example, in Ref. 27, NSNLs in non-centrosymmetric spinful systems are systematically discussed. Unlike ours, their NSNLs appear between high-symmetry points and high-symmetry lines or between high-symmetry points. Therefore, NSNLs are not fixed at four-fold degenerate points, unlike those in the spinless systems in our theory. We also note that in Ref. 28 and Ref. 29, NSNLs in spinful systems with the space group No.**62** are discussed and applied to materials, $SrIrO_3$ and CaGaPt, respectively. Because $SrIrO_3$ and CaGaPt have strong spin-orbit coupling, the positions of their NSNLs are different from our theory.

Recent papers discuss band structures which cannot be realized as an atomic limit.[35,36] In contrast, the present paper discusses symmetry-enforced nodal lines, which appear regardless of whether the band structure is realized as an atomic limit or not, and is different from these previous studies.

ACKNOWLEDGMENTS

We are grateful to H. Watanabe and M. Yamada for useful comments. This work was supported by the Grant-in-Aid for Scientific Research (numbers 26287062 and 16K13834), and by the MEXT Elements Strategy Initiative to Form Core Research Center (TIES).

Appendix A: Direct calculation of irreducible representation for orthorhombic space groups

From our result in Sec. II, NSNLs enforced by symmetry appear with four-fold degeneracy. Here, we explain how four-fold degeneracy in orthorhombic primitive space groups appears.

We consider orthorhombic systems with the following space-group symmetries:

$$
\begin{aligned}
P &= \left\{ \begin{pmatrix} -1 & & \\ & -1 & \\ & & -1 \end{pmatrix} \;\middle|\; \begin{pmatrix} 0 \\ 0 \\ 0 \end{pmatrix} \right\}, \\
G_1 &= \left\{ \begin{pmatrix} -1 & & \\ & -1 & \\ & & 1 \end{pmatrix} \;\middle|\; \frac{1}{2}\mathbf{d}_1 \right\}, \\
G_2 &= \left\{ \begin{pmatrix} -1 & & \\ & 1 & \\ & & -1 \end{pmatrix} \;\middle|\; \frac{1}{2}\mathbf{d}_2 \right\},
\end{aligned} \tag{A1}
$$

where $\mathbf{d}_i = \sum_\alpha d_i^\alpha \mathbf{a}^\alpha (i = 1, 2)$ ($d_i^\alpha = 0, 1$) is a linear combination of the primitive vectors $\mathbf{a}^\alpha (\alpha = x, y, z)$, and we set the lengths of the vectors $\mathbf{a}^\alpha$ to be unity. P represents the inversion operation. G_1 and G_2 represent 2-fold screw rotations. Therefore PG_1 and PG_2 are glide reflections. Commutation relations among P, G_1, G_2 are as follows:

$$P^2 = E, \quad G_1^2 = T_z^{d_1^z}, \quad G_2^2 = T_y^{d_2^y}, \tag{A2}$$

$$G_1 P = T_x^{d_1^x} T_y^{d_1^y} T_z^{d_1^z} P G_1, \tag{A3}$$

$$G_2 P = T_x^{d_2^x} T_y^{d_2^y} T_z^{d_2^z} P G_2, \tag{A4}$$

$$G_1 G_2 = T_x^{(d_1^x - d_2^x)} T_y^{-d_2^y} T_z^{d_1^z} G_2 G_1. \tag{A5}$$

Here, $T_{x,y,z}$ are the unit translation operators in the x, y, z directions, respectively. These complicated relations become simpler at the TRIM, because $T_x, T_y, T_z = \pm 1$ at TRIM. Therefore, we only need to calculate the following $2^5 = 32$ patterns:

$$G_1^2 = (-1)^{\delta_A}, \; G_2^2 = (-1)^{\delta_B}, \tag{A6}$$

$$G_1 P = (-1)^{\delta_C} P G_1, \tag{A7}$$

$$G_2 P = (-1)^{\delta_D} P G_2, \tag{A8}$$

$$G_1 G_2 = (-1)^{\delta_E} G_2 G_1. \tag{A9}$$

Here, $\delta_{A,\cdots,E}$ are either 0 or 1, and their values are determined from the momentum $k_{x,y,z} = 0, \pi$ and the values of $d_{1,2}^{x,y,z} = 0, 1$ as follows:

$$\delta_A = \frac{k_z}{\pi} d_1^z, \delta_B = \frac{k_y}{\pi} d_2^y, \tag{A10}$$

$$\delta_C = \frac{k_x}{\pi} d_1^x + \frac{k_y}{\pi} d_1^y + \frac{k_z}{\pi} d_1^z, \tag{A11}$$

$$\delta_D = \frac{k_x}{\pi} d_2^x + \frac{k_y}{\pi} d_2^y + \frac{k_z}{\pi} d_2^z, \tag{A12}$$

$$\delta_E = \frac{k_x}{\pi} (d_1^x - d_2^x) - \frac{k_y}{\pi} d_2^y + \frac{k_z}{\pi} d_1^z. \tag{A13}$$

Once the commutation relations are given, we can calculate whether four-fold degeneracy appears at each high-symmetry point; the result is listed on Table II. Here, we take into account that the time-reversal symmetry satisfies $\Theta^2 = \mathbf{1}$ in spinless systems.

For example, $((-1)^{\delta_A}, \cdots, (-1)^{\delta_E}) = (- + + - +)$ at the T point in the space group $Pbcn$ (No.**60**). In this case, P and G_2 anti-commute. Here, we introduce real matrices Γ_1 and Γ_2 with the following properties:

$$\Gamma_1^2 = \Gamma_2^2 = 1, \quad \Gamma_1 \Gamma_2 = -\Gamma_2 \Gamma_1. \tag{A14}$$

P and G_2 can be represented by Γ_1 and Γ_2, respectively. G_1 commutes with P and with G_2, and $G_1^2 = -\mathbf{1}$. Therefore, irreducible representations of this group are represented by the following:

$$P = \Gamma_1, \quad G_1 = \pm i\mathbf{1}, \quad G_2 = \Gamma_2. \tag{A15}$$

If time-reversal symmetry is absent, we obtain two different two-dimensional irreducible representations with different signs of G_1. For example, they are represented by the Pauli matrices $\tau_{x,y,z}$ as follows: $P = \tau_z$, $G_1 = \pm i\mathbf{1}$, $G_2 = \tau_x$. In our case, time-reversal symmetry is preserved. Because eigenvalues of G_1 are pure imaginary, their signs are flipped by time-reversal operation. Therefore, two irreducible representations are related by time-reversal symmetry, and become a 4-dimensional corepresentation. For example, based on the eigenstates of P and G_1, they are represented as follows:

$$P = \tau_z, \quad G_1 = i\mu_z, \quad G_2 = \tau_x, \quad \Theta = \mu_x K, \tag{A16}$$

where μ_i are the Pauli matrices. If we include a spin degree of freedom, we use tensor product with the spin matrices. In our case, the representation is given by

$$P = \tau_z,\ G_1 = i\mu_z \otimes i\sigma_z,\ G_2 = \tau_x \otimes i\sigma_y, \\ \Theta = \mu_x \otimes i\sigma_y K. \tag{A17}$$

This representation is not irreducible, but can be reduced to two irreducible representations. In this case, PG_1 commutes with all elements. Therefore, two irreducible representations are distinguished by the eigenvalues of PG_1. So far, we have discussed irreducible representations at high-symmetry points. Irreducible representations at high-symmetry lines are also calculated by similar discussion. The only difference is that the number of symmetry operations is reduced because the symmetry is lower.

Space group	$\boldsymbol{k}$-point	$((-1)^{\delta_A}, \cdots, (-1)^{\delta_E})$
52 *Pnna*	S	$(+--+-)$
54 *Pcca*	U	$(++---)$
	R	$(++---)$
56 *Pccn*	U	$(++---)$
	T	$(+--+-)$
57 *Pbcm*	T	$(---++)$
	R	$(---++)$
60 *Pbcn*	U	$(-+++-+)$
	T	$(-+++-+)$
	R	$(-+--+)$
61 *Pbca*	U	$(-+++-+)$
	S	$(+---+)$
	T	$(---++)$
	R	$(--++-)$
62 *Pnma*	S	$(+---+)$
	R	$(--+--)$

TABLE II. List of orthorhombic space groups which have a four-dimensional irreducible representation at a high symmetry point. The first column shows the numbers and the short symbols of the space groups. The second column shows the $\boldsymbol{k}$-points with 4-fold degeneracy. The third column shows the signs of $(-1)^{\delta_i}$ $(i = A, \cdots, E)$.

Appendix B: Direct calculation of irreducible representations for tetragonal space groups

We can extend our calculation in Appendix A to tetragonal space groups. In tetragonal space groups, we have the following three symmetries:

$$P = \left\{ \begin{pmatrix} -1 & & \\ & -1 & \\ & & -1 \end{pmatrix} \middle| \begin{pmatrix} 0 \\ 0 \\ 0 \end{pmatrix} \right\}, \\ \tilde{G}_1 = \left\{ \begin{pmatrix} & -1 & \\ 1 & & \\ & & 1 \end{pmatrix} \middle| \frac{1}{2}\mathbf{d}_1 \right\}, \\ G_2 = \left\{ \begin{pmatrix} -1 & & \\ & 1 & \\ & & -1 \end{pmatrix} \middle| \frac{1}{2}\mathbf{d}_2 \right\}. \tag{B1}$$

where $\mathbf{d}_i = \sum_\alpha d_i^\alpha \mathbf{a}^\alpha (i = 1, 2)$ $(d_i^\alpha = 0, 1)$ is a linear combination of the Bravais lattice vector $\mathbf{a}^\alpha (\alpha = x, y, z)$, and P, G_2 are the same with the orthorhombic cases. $\tilde{G}_1$ represents the four-fold screw rotation, which is absent in orthorhombic space groups. By calculating commutation relations between $P, \tilde{G}_1, G_2$, we can calculate irreducible representations at TRIM in the similar way as in orthorhombic space groups.

Commutation relations of $P, \tilde{G}_1, G_2$ are as follows:

$$P^2 = E, \quad \tilde{G}_1^4 = T_z^{2d_1^z}, \quad G_2^2 = T_y^{d_2^y}, \tag{B2}$$

$$\tilde{G}_1 P = T_x^{d_1^x} T_y^{d_1^y} T_z^{d_1^z} P \tilde{G}_1, \tag{B3}$$

$$G_2 P = T_x^{d_2^x} T_y^{d_2^y} T_z^{d_2^z} P G_2, \tag{B4}$$

$$\tilde{G}_1^2 P = T_x^{d_1^x - d_1^y} T_y^{d_1^x + d_1^y} T_z^{2d_1^z} P \tilde{G}_1^2, \tag{B5}$$

$$\tilde{G}_1 G_2 \tilde{G}_1 = T_x^{(d_1^x - d_1^y - d_2^x - d_2^y)/2} T_y^{(-d_1^x + d_1^y + d_2^x - d_2^y)/2} G_2, \tag{B6}$$

$$\tilde{G}_1^2 G_2 = T_x^{d_1^x - d_1^y - d_2^x} T_y^{-d_2^y} G_2 \tilde{G}_1^2. \tag{B7}$$

We can simplify these relations at high-symmetry points Γ, Z, M and A, because $T_x, T_y, T_z = \pm 1$ and $T_x = T_y$ at these points. For other TRIM, R and X, we can calculate similarly as in the orthorhombic case, because they do not have four-fold screw symmetry.

At the high-symmetry points Γ, Z, M and A, because $T_x = T_y$, Eqs. (B3)-(B7) become:

$$\tilde{G}_1 P = T_x^{d_1^x + d_1^y} T_z^{d_1^z} P \tilde{G}_1, \tag{B8}$$

$$G_2 P = T_x^{d_2^x + d_2^y} T_z^{d_2^z} P G_2, \tag{B9}$$

$$\tilde{G}_1^2 P = P \tilde{G}_1^2, \tag{B10}$$

$$\tilde{G}_1 G_2 \tilde{G}_1 = T_x^{-d_2^y} G_2, \tag{B11}$$

$$\tilde{G}_1^2 G_2 = T_x^{d_1^x - d_1^y - d_2^x - d_2^y} G_2 \tilde{G}_1^2. \tag{B12}$$

Because $T_x, T_y, T_z = \pm 1$ at highest-symmetry points, the factors in the r.h.s of Eqs. (B8)-(B12) involving T_i are either $+1$ or -1. Therefore, $T_x^{-d_2^y}$ in Eq. (B11) is equal to $G_2^2 = T_y^{d_2^y}$.

From the last two equations, we obtain

$$\tilde{G}_1^2 G_2 \tilde{G}_1^2 = T_x^{-2d_2^y} G_2, \tag{B13}$$

$$\tilde{G}_1^2 G_2 \tilde{G}_1^2 = T_x^{d_1^x - d_1^y - d_2^x - d_2^y} G_2 \tilde{G}_1^4 = T_x^{d_1^x - d_1^y - d_2^x - d_2^y} G_2. \tag{B14}$$

Therefore, the factor involving T_x in the right-hand side of Eq. (B12) only takes the positive sign.

We calculate the following $2^3 = 8$ patterns:

$$G_2^2 = (-1)^{\delta_A} E, \tilde{G}_1 P = (-1)^{\delta_B} P \tilde{G}_1, G_2 P = (-1)^{\delta_C} P G_2. \tag{B15}$$

where $\delta_{A,\cdots,C}$ are either 0 or 1, determined from the momentum $k_{x,y,z} = 0, \pi$ and the values of $d_{1,2}^{x,y,z} = 0, 1$ are as follows:

$$\delta_A = \frac{k_y}{\pi} d_2^y, \tag{B16}$$

$$\delta_B = \frac{k_x}{\pi} d_1^x + \frac{k_y}{\pi} d_1^y + \frac{k_z}{\pi} d_1^z, \tag{B17}$$

$$\delta_C = \frac{k_x}{\pi} d_2^x + \frac{k_y}{\pi} d_2^y + \frac{k_z}{\pi} d_2^z, \tag{B18}$$

By a direct calculation, we can determine whether a four-fold degenerate point can appear. There are 2 cases: (a) only four-fold degenerate irreducible representations exist, or (b) 2-fold degenerate irreducible representations are also possible. Symmetry-enforced NSNLs require the case (a), as a result of calculation for all the possible space group. By these considerations, we obtain the list in Sec. Ⅲ B.

[1] C. L. Kane and E. J. Mele, Phys. Rev. Lett. **95**, 146802 (2005).
[2] C. L. Kane and E. J. Mele, Phys. Rev. Lett. **95**, 226801 (2005).
[3] B. A. Bernevig and S.-C. Zhang, Phys. Rev. Lett. **96**, 106802 (2006).
[4] B. A. Bernevig, T. L. Hughes, and S.-C. Zhang, Science **314**, 1757 (2006).
[5] M. Z. Hasan and C. L. Kane, Rev. Mod. Phys. **82**, 3045 (2010).
[6] X.-L. Qi and S.-C. Zhang, Rev. Mod. Phys. **83**, 1057 (2011).
[7] M. König *et al.*, Science **318**, 766 (2007).
[8] H. Zhang *et al.*, Nat. Phys. **5**, 438 (2009).
[9] Y. Chen *et al.*, Science **325**, 178 (2009).
[10] L. Fu, Phys. Rev. Lett. **106**, 106802 (2011).
[11] T. H. Hsieh *et al.*, Nat. Commun. **3**, 982 (2012).
[12] Y. Tanaka *et al.*, Nat. Phys. **8**, 800 (2012).
[13] P. Dziawa *et al.*, Nat. Mater. **11**, 1023 (2012).
[14] S. Y. Xu *et al.*, Nat. Commun. **3**, 1192 (2012).
[15] A. A. Burkov, M. D. Hook, and L. Balents, Phys. Rev. B **84**, 235126 (2011).
[16] S. Murakami, New J. Phys. **9**, 356 (2007).
[17] Z. Liu *et al.*, Science **343**, 864 (2014).
[18] S.-Y. Xu *et al.*, Science **349**, 613 (2015).
[19] H. Weng, X. Dai, and Z. Fang, J. Phys.: Condens. Matter **28**, 303001 (2016).
[20] L. S. Xie *et al.*, APL Mater. **3**, 083602 (2015).
[21] Y. Kim, B. J. Wieder, C. L. Kane, and A. M. Rappe, Phys. Rev. Lett. **115**, 036806 (2015).
[22] A. Yamakage, Y. Yamakawa, Y. Tanaka, and Y. Okamoto, J. Phys. Soc. Jpn. **85**, 013708 (2016).
[23] L. M. Schoop *et al.*, Nat. Commun. **7** (2016).
[24] Y.-H. Chan, C.-K. Chiu, M. Y. Chou, and A. P. Schnyder, Phys. Rev. B **93**, 205132 (2016).
[25] M. Hirayama, R. Okugawa, T. Miyake, and S. Murakami, Nat. Commun. **8**, 14022 (2017).
[26] R. Yu, Z. Fang, X. Dai, and H. Weng, Front. Phys. **12**, 127202 (2017).
[27] T. Bzdušek, Q. Wu, A. Rüegg, M. Sigrist, and A. A. Soluyanov, Nature **538**, 75 (2016).
[28] Y. Chen, H.-S. Kim, and H.-Y. Kee, Phys. Rev. B **93**, 155140 (2016).
[29] R. Chen, H. C. Po, J. B. Neaton, and A. Vishwanath,

arXiv preprint arXiv:1611.06860 (2016).
[30] M. I. Aroyo, A. Kirov, C. Capillas, J. M. Perez-Mato, and H. Wondratschek, Acta Crystallogr. Sect. A **62**, 115 (2006).
[31] B. J. Wieder, Y. Kim, A. M. Rappe, and C. L. Kane, Phys. Rev. Lett. **116**, 186402 (2016).
[32] H. Watanabe, H. C. Po, M. P. Zaletel, and A. Vishwanath, Phys. Rev. Lett. **117**, 096404 (2016).
[33] `http://www.openmx-square.org/`.
[34] C. Gueneau, C. Servant, F. d'Yvoire, and N. Rodier, Acta Crystallogr. Sect. C **51**, 177 (1995).
[35] H. C. Po, A. Vishwanath, H. Watanabe, arXiv preprint arXiv:1703.00911 (2017).
[36] B. Bradlyn, L. Elcoro, J. Cano, M. G. Vergniory, Z. Wang, C. Felser, M. I. Aroyo, B. A. Bernevig, arXiv preprint arXiv:1703.02050 (2017).